AN IMPROVED DISCRETE MODEL FOR THREE-PHASE VOLTAGE-FED SPACE VECTOR MODULATED CONVERTERS

F. Botterón, H. Pinheiro, H. A. Gründling, J. R. Pinheiro, H. L. Hey
Power Electronics and Control Research Group – GEPOC
Federal University of Santa Maria – UFSM - 97105-900 – Santa Maria, RS – Brazil
fer_bot@mixmail.com, humberto@ctlab.ufsm.br

Abstract – **This paper proposes a non-linear discrete large signal model for space vector modulated three-phase converters. This model take into account the switching sequence, sampling instants and switching frequency. In addition, this discrete non-linear model does not require that the ripple over the variables to be small. Furthermore, two average linear models are compared. The proposed linear model, by least square approximation, results in better approximation for lower ratios of the switching and fundamental frequency. Simulation results are presented in the paper.**

KEYWORDS

Discrete Models. Modeling and Control. Space Vector Modulated Converters.

I. INTRODUCTION

In the design of the three-phase PWM converters for uninterruptible power supplies (UPS) and active filters, there are two main steps: (i) the choice of the modulation strategy and filters design, and (ii) the controllers design to achieve a predefined dynamic performance. Regarding the choice of the modulation strategy, several techniques, differing in concept and performance, have been developed in the last decades. Among them, space vector modulation has been increasingly used [1-5], because it allows reducing the commutation losses and/or the harmonic content of the voltage (or currents), as well as to obtain higher amplitude modulation indexes if compared with conventional techniques[1,2]. Moreover, space vector modulation can be easily implemented in digital processors, [3,4,5]. Once defined the modulation technique and the filter design, the controller design for the closed-loop operation can be performed. Related to the controller implementation, it is important to point out that digital control techniques for three-phase PWM converters are widely used. On the one hand, due to the well-known advantages of the digital controls in terms of flexibility to upgrade and easy of implementation, and on the other hand, due to availability of relatively low cost microcontrollers and digital signal processors (DSP) with dedicate peripherals to control static converters.

The first step for the controller design is to derive a dynamic model. Several papers on the literature deal with continuous dynamic models for three-phase PWM converters. In [6], average and small-signal models for three-phase PWM converters are presented, in stationary and rotating coordinates. This average model assumes that the control inputs vary slowly relative to the switching frequency, as well as that the ripple over the variables of the interest are negligible. Therefore, its validity is restricted to the frequency ranges significantly smaller than the converter switching frequency.

On the other hand, [7] proposes equivalent circuits for the three-phase converters and filters in rotating *dq* coordinates using time-varying ideal transformers, where their transformation ratios are equal to the switches duty ratios and a "gyrator" is introduced, to take into account the resulting crosscoupling between the *dq* axes. From these equivalents circuits, is simple to find a steady state operating point as well as the small-signal input to output transfer functions. Afterward, a systematic approach to small-signal modeling three-phase PWM converters is proposed in [8]. Transfer functions useful for the controller design in the continuous time-domain are derived from the small-signal models obtained by the linearization of the large-signal model at an operating point, assuming again that the ripple variables due to the switching are negligible. In [8], the authors investigate the effects of the controller digital implementation and the discrete nature of the PWM modulation, which has been taken into account through a ZOH on the inductor currents. However, it is important to note that this continuous-time model only describe the converter operating for balanced three-phase systems. Subsequently, in [9] a small-signal model for a space vector modulated converter for two specific switching sequences, have been proposed. This model reveals that the modulator introduces not only a gain, but also time-varying delays and additional crosscoupling into the control inputs when the system is representing in rotating *dq* coordinates. On the other hand, a reduced order small-signal model for three-phase PWM rectifiers is proposed in [10], where the six-step PWM modulator [11] is used. Again, this continuous-time model is valid for this considered modulation and it is inadequate for discrete-time controllers design.

Discrete-models are preferred over continuous models since the delays of the digital implementation can be easily modeled and the resulting controller is in an adequate form for its implementation. Large-signals average discrete-models have been widely used for controller design of the three-phase PWM converters, [12-17]. These models are obtained by approximating the three-phase PWM converter by a ZOH, and then, solving the linear time-invariant state-space equation associated with the filter and load, along of one discretization period [12,14,16,17].

These discrete models, in a similar way as the large-signal average continuous model [6], are independent of the operating point, and they consider that the ripples over the variables of the interest are small. However, its validity range, still not well defined, and the impact of the sampling, modulation strategy and filter cut-off frequency, (on the voltages and currents using for feedback), have not been

reported in the literature. Moreover, an additional aggravating appear in medium and high power applications, where the switching frequency is low to limit the switching losses. As a result, low-order harmonics on the sampled variables can appear, depending on the modulation strategy and/or the sampling instants. These phenomena can occur as well, when the filters are light, making the ripple over the controlled signals more significant. It is important to point out that neither previous model describes those phenomena. The direct utilization of the measurements values containing harmonics, to compute the control law, degrades the system performance [1,18,19]. Therefore, to achieve a good performance, its required that the measurement values appear without harmonics. Some techniques to avoid the harmonics into measured variables have been proposed. One is the method of instantaneous sampling, which suggests that it is possible to detect the fundamental component of a current, by sampling it at the midpoint of the zero vectors, when a space vector modulation with a symmetric switching sequence is utilized, [18,19], or in the peaks of the triangular carrier of the conventional comparison method [18]. Another technique employs a low-pass filter in the measured variables, and then, samples the filtered variables [18]. This technique requires an additional hardware and introduces delay on the sampled variables. Attempts to compensate the additional dynamic of the filter by delaying the sampling instants have been presented in [19]. However, this technique increases the hardware complexity, and noises sensitivity. For example, if a sampling is performed during a commutation. It is worth to mention that the above-mentioned efforts to eliminate harmonics on the measured variables are restricted to the inverter for motor drives applications, where the controlled plant can be approximated by a first order model. In addition, the impact of utilizes different switching sequences and sampling strategies have not been investigated.

The focus of this paper is to investigate the impact of the different switching sequences, as well as different sampling strategies in digitally controlled three-phase PWM converters for UPS applications. A large-signal non-linear discrete model of the three-phase voltage-fed space vector modulated converter is proposed. This discrete model is compared with the linear model obtained by the approximation of the PWM converter by a ZOH. The impact of the switching frequency, sampling, cut-off filter frequency as well as the switching sequences is investigated in details.

II. CONTINUOUS NORMALIZED MODEL OF THE OUTPUT FILTER AND LOAD

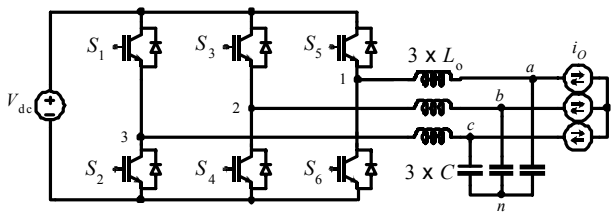

Fig. 1 – Three-phase Inverter and LC filter

A. State-space continuous model in stationary abc frame

A typical three-phase voltage source inverter with LC filter and load found in UPS applications is shown in Fig. 1. The DC link voltage usually has low impedance and can be considered as an ideal voltage source. On the other hand, the output LC filter and load can be modeled by the following state-space equation, where the load is considered as disturbances, that is:

$$\dot{\mathbf{x}}(t) = \mathbf{A}\,\mathbf{x}(t) + \mathbf{B}\,\mathbf{u}(t) + \mathbf{F}\,\mathbf{w}(t) \qquad (1)$$

The matrices **A**, **B**, **F** in (1), can be found in the Appendix, and the vectors **x**, **u** and **w** have been selected as:

$$\mathbf{x} = \begin{bmatrix} i_a & i_b & i_c & v_a & v_b & v_c \end{bmatrix}^{\mathrm{T}},\ \mathbf{u} = \begin{bmatrix} u_{12pwm} & u_{23pwm} \end{bmatrix}^{\mathrm{T}},$$

$$\mathbf{w} = \begin{bmatrix} i_{oa} & i_{ob} & i_{oc} \end{bmatrix}^{\mathrm{T}}$$

Aiming to limit the dynamic range of variables for a fixed-point implementation of the controller, a linear transformation that normalizes the circuit variable is applied to (1). By choosing the base values, the normalized voltage and current variables can be written as: $v_n = \frac{v}{V_{base}}$, $i_n = \frac{i}{I_{base}}$.

Now, defining a normalizing linear transformation $\mathbf{T}_n$ as a diag($1/I_{base}$ $1/I_{base}$ $1/I_{base}$ $1/V_{base}$ $1/V_{base}$ $1/V_{base}$), the normalized state, input and disturbance vectors become:

$$\mathbf{x_n}(t) = \mathbf{T_n}\mathrm{x}(t)\ ,\ \mathbf{u}(t) = V_{base}\mathbf{u_n}(t)\ ,\ \mathbf{w}(t) = I_{base}\mathbf{w_n}(t)$$

As a result the state equation (1) can be written in a compact form as (2),

$$\dot{\mathbf{x}}_\mathbf{n}(t) = \mathbf{T_n}\mathbf{A}\mathbf{T_n}^{-1}\mathbf{x_n}(t) + \mathbf{T_n}\mathbf{B}V_{base}\mathbf{u_n}(t) + \mathbf{T_n}\mathbf{F}I_{base}\mathbf{w_n}(t)\ . \qquad (2)$$

B. State-space continuous model in rotating dq frame

By representing (2) into the αβ frame and then in the rotating *dq* frame, see (A2) and (A3) in Appendix, the state-space normalized continuous model of the LC filter and load is obtained, as described by (3).

where, the matrices $\mathbf{A}_{dq}$, $\mathbf{B}_{dq}$ and $\mathbf{F}_{dq}$ are given in (A4) and, $\mathbf{x}_{dq} = \begin{bmatrix} v_d & v_q & i_d & i_q \end{bmatrix}^{\mathrm{T}}$, $\mathbf{u}_{dq} = \begin{bmatrix} u_{d\,pwm} & u_{q\,pwm} \end{bmatrix}^{\mathrm{T}}$, $\mathbf{w}_{dq} = \begin{bmatrix} I_{od} & I_{oq} \end{bmatrix}^{\mathrm{T}}$.

Note that equation (3) is a normalized continuous model where $u_{d\ pwm}$ and $u_{q\ pwm}$ are the voltages produced by the inverter represented in the rotating *dq* frame.

$$\dot{\mathbf{x}}_{dq}(t) = \mathbf{A}_{dq}\mathbf{x}_{dq}(t) + \mathbf{B}_{dq}\mathbf{u}_{dq}(t) + \mathbf{F}_{dq}\mathbf{w}_{dq}(t)\,, \qquad (3)$$

In order to obtain a discrete-time model, the equation (3) must be solved from the beginning to the end of a sampling period T. Fig. 2, shows a block diagram representation of a three-phase PWM inverter with the discrete control action generated in the *dq* frame. It is assumed that the sampling and updating control laws are equal. Typical waveforms of $u_{d\ pwm}$ and $u_{q\ pwm}$ are shown in Fig. 3. It is possible to see, that these voltages depend on the discrete control actions $u_d(k\mathrm{T})$ and $u_q(k\mathrm{T})$ as well as the inverter modulation technique. In the next section, it is derived a discrete average state-space model, which is often used in the design of the discrete-time controller for the three-phase PWM inverters.

III. THREE-PHASE PWM INVERTER DISCRETE AVERAGE STATE-SPACE MODEL

In order to obtain the discrete average state-space model for the three-phase PWM inverter, the following assumptions are required: (i) the sampling frequency is much higher that the fundamental frequency; (ii) the ripple over the sampled variables are negligible or they are sampled at their mean values.

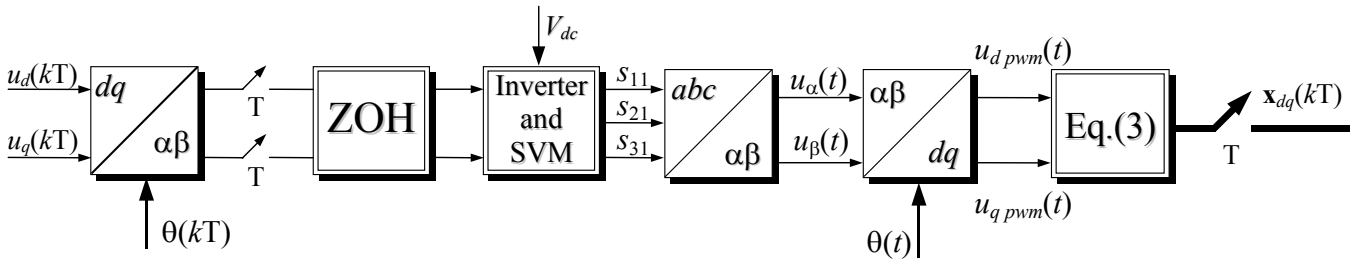

Fig. 2. – Block diagram representation of three-phase SVM inverter model in rotating *dq* frame.
ZOH: zero-order hold, **SVM**: Space Vector Modulator. **T**: Sampling Period.

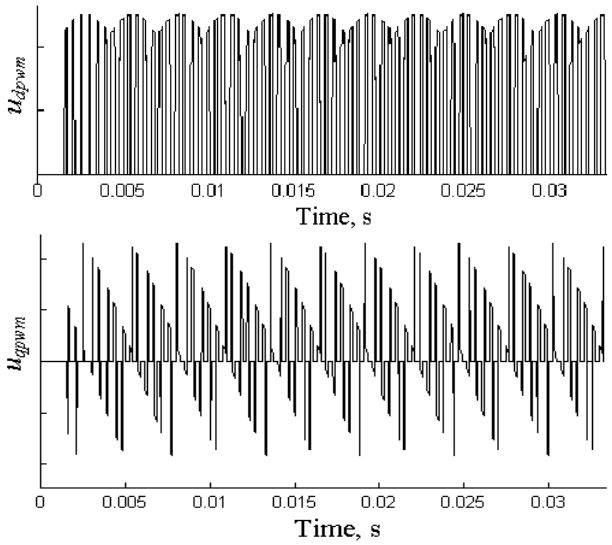

Fig. 3 – Typical PWM output voltages produced by the three-phase inverter in the rotating *dq* frame. From top to bottom $u_{d\,pwm}$, $u_{q\,pwm}$

With (i), θ(*k*T) is almost constant in a sampling period, allowing the discrete *dq*-αβ transformation and the continuous αβ-*dq* transformation to be canceled out. The second assumption is required since $u_{d\ pwm}$ and $u_{q\ pwm}$ are pulsed voltages, as shown in Fig. 3. As a result the sampled vector $\mathbf{x}_{dq}(k\mathrm{T})$ may be different from their average value in a sampling period.

If the assumptions made are valid, $u_{d\ pwm}$ and $u_{q\ pwm}$ can be represented by their average value in a sampling period. As a result a discrete linear time invariant model is obtained by solving (3) in one sampling period, that is,

$$\mathbf{x}_{dq}((k+1)\mathrm{T}) = e^{\mathbf{A}_{dq}\mathrm{T}}\mathbf{x}_{dq}(k\mathrm{T}) + \int_0^{\mathrm{T}} e^{\mathbf{A}_{dq}(\mathrm{T}-\tau)}d\tau\,\mathbf{B}_{dq}\,\mathbf{u}_{dq}(k\mathrm{T}), \quad (4)$$

or in a compact form,

$$\mathbf{x}_{dq}(k+1) = \mathbf{G}\,\mathbf{x}_{dq}(k) + \mathbf{H}\,\mathbf{u}_{dq}(k), \quad (5)$$

where: $\mathbf{G} = e^{\mathbf{A}_{dq}\mathrm{T}}$ and $\mathbf{H} = \mathbf{A}_{dq}^{-1}\left[e^{\mathbf{A}_{dq}\mathrm{T}} - \mathbf{I}\right]\mathbf{B}_{dq}$, if the inverse of $\mathbf{A}_{dq}$ exist. The linear parameters used later to comparing, are defined as: $[H_1 \quad H_2 \quad H_3 \quad H_4]^{\mathrm{T}} = \mathbf{H}\,\mathbf{u}_{dq}(k\mathrm{T})$.

As a result of the above simplifications the block diagram of Fig. 2 is rendered to the one shown in Fig. 4.

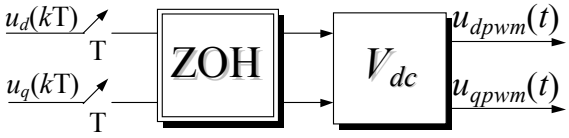

Fig. 4 – Simplified block diagram representation of the three-phase SVM inverter.

If the assumptions made at the beginning of this section are violated, a non-linear discrete model should be considered to describe the relationship between the input and output variables of three-phase PWM inverter in the rotating frame. Next section derives this model and later, the range of validity of the average discrete model SVM inverter (5) is investigated.

IV. THREE-PHASE SVM INVERTER LARGE-SIGNAL NON-LINEAR DISCRETE STATE-SPACE MODEL

This section develops a discrete-time large-signal non-linear model of the SVM three-phase inverter. Lets us consider the block diagram representation of the SVM three-phase inverter of Fig. 5. In this block diagram, the discrete rotating *dq* to stationary αβ frame transformation, is defined as:

$$\begin{aligned} u_\alpha(k\mathrm{T}) &= u_d(k\mathrm{T})\cos(\theta(k\mathrm{T})) - u_q(k\mathrm{T})\,\mathrm{sen}(\theta(k\mathrm{T})), \\ u_\beta(k\mathrm{T}) &= u_d(k\mathrm{T})\,\mathrm{sen}(\theta(k\mathrm{T})) + u_q(k\mathrm{T})\cos(\theta(k\mathrm{T})). \end{aligned} \quad (6)$$

From the control actions $u_\alpha(k\mathrm{T})$ and $u_\beta(k\mathrm{T})$, the duration times of each non-zero switching vectors can be determined as:

$$\begin{bmatrix} t_1(k\mathrm{T}) \\ t_2(k\mathrm{T}) \end{bmatrix} = \mathrm{T}_{pwm}\mathbf{M}_i^{-1}\begin{bmatrix} u_\alpha(k\mathrm{T}) \\ u_\beta(k\mathrm{T}) \end{bmatrix}, \quad (7)$$

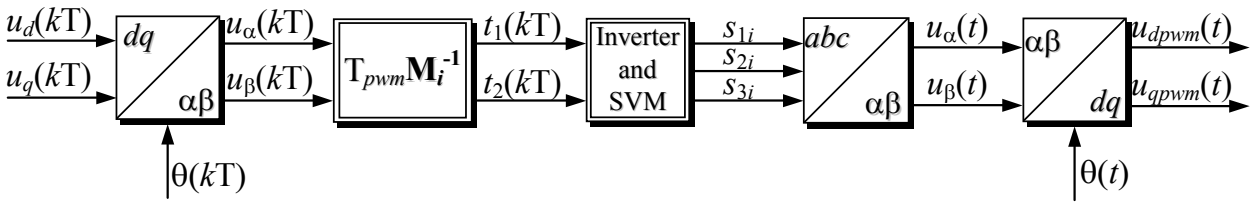

Fig. 5 - Blocks diagram of the SVM three-phase inverter

where $\mathbf{M}_i$, is the decomposition matrix associated with the sector i, for i = 1,...,6. Alternatively, the time durations of each switching vectors, can be expressed as in (8) and (9).

$$t_1(k\mathrm{T}) = \mathrm{T}_{pwm}\langle \mathbf{m_{11}}, \mathbf{T}_{dq}(\theta(k\mathrm{T}))\mathbf{u}_{dq}(k\mathrm{T})\rangle\,, \tag{8}$$

$$t_2(k\mathrm{T}) = \mathrm{T}_{pwm}\langle \mathbf{m_{21}}, \mathbf{T}_{dq}(\theta(k\mathrm{T}))\mathbf{u}_{dq}(k\mathrm{T})\rangle\,, \tag{9}$$

where $\mathbf{m}_{11}$ and $\mathbf{m}_{21}$ are rows of the $\mathbf{M}_i$ matrix.

These duration times and their distribution along of a switching period are shows in Fig. 6, where symmetric switching sequence along the sector 1, is considered.

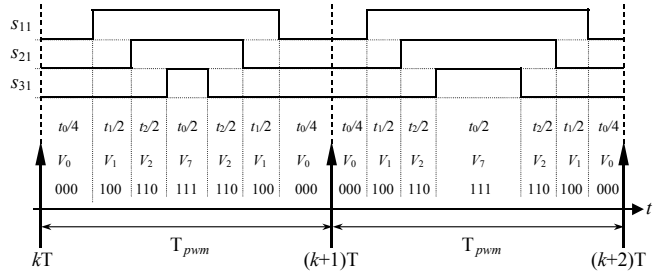

Fig. 6 – Symmetric space vector modulation pattern in *abc* coordinates for the sector 1.

By considering the symmetric switching sequence of Fig. 6, the PWM phase voltage produced by the inverter, can be expressed as

$$s_{1i} = g_{1i}(u_d(k\mathrm{T}), u_q(k\mathrm{T}), \theta(k\mathrm{T}), t)\,, \tag{10}$$

$$s_{2i} = g_{2i}(u_d(k\mathrm{T}), u_q(k\mathrm{T}), \theta(k\mathrm{T}), t)\,, \tag{11}$$

$$s_{3i} = g_{3i}(u_d(k\mathrm{T}), u_q(k\mathrm{T}), \theta(k\mathrm{T}), t)\,, \tag{12}$$

where, g_{1i}, g_{2i} e g_{3i} are time-variant and non-linear scalar functions in stationary *abc* frame. Therefore, PWM continuous time inverter output voltages in stationary $\alpha\beta$ frame and in the rotating *dq* frame, can be expressed as,

$$\begin{bmatrix} u_\alpha(t) \\ u_\beta(t) \end{bmatrix} = \mathbf{T}_{\alpha\beta}\begin{bmatrix} s_{1i} \\ s_{2i} \\ s_{3i} \end{bmatrix} \Rightarrow \begin{bmatrix} u_{dpwm}(t) \\ u_{qpwm}(t) \end{bmatrix} = \mathbf{T}_{dq}(\theta(t))\begin{bmatrix} u_\alpha(t) \\ u_\beta(t) \end{bmatrix}, \tag{13}$$

where, $\mathbf{T}_{\alpha\beta}$ and $\mathbf{T}_{dq}(\theta(t))$, are given in Appendix. Aiming to obtain a compact representation, the continuous time inverter output voltages in rotating *dq* frame can be written in the following form:

$$\mathbf{u}_{dq} = \begin{bmatrix} u_{dpwm}(t) \\ u_{qpwm}(t) \end{bmatrix} = \begin{bmatrix} g_{di}(u_d(k\mathrm{T}), u_q(k\mathrm{T}), \theta(k\mathrm{T}), \theta(t), t) \\ g_{qi}(u_d(k\mathrm{T}), u_q(k\mathrm{T}), \theta(k\mathrm{T}), \theta(t), t) \end{bmatrix}. \tag{14}$$

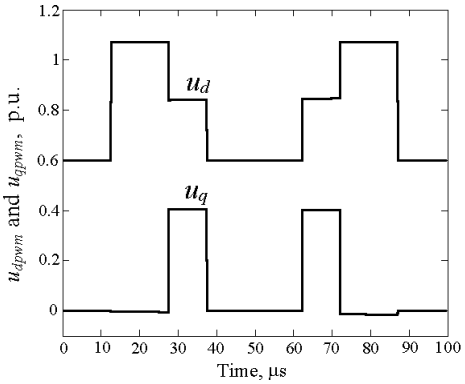

Fig. 7 – PWM voltages in rotating *dq* frame for the sector 1.

The equation (14) can be used to obtain the non-linear discrete state-space model of the SVM inverter. This is accomplish by solving (3) from the beginning to the end of a sampling interval, that is,

$$\mathbf{x}_{dq}((k+1)\mathrm{T}) = e^{\mathbf{A}_{dq}\mathrm{T}}\mathbf{x}_{dq}(k\mathrm{T}) + \int_{k\mathrm{T}}^{(k+1)\mathrm{T}} e^{\mathbf{A}_{dq}((k+1)\mathrm{T}-\tau)}\mathbf{B}_{dq}\,\mathbf{u}_{dq}(\cdot,\tau)d\tau\,. \tag{15}$$

where $\mathbf{u}_{dq}(.,\tau)$ is given by (14) and typical waveform of its entries are showed in Fig. 7. The equation (15) can also be expressed as,

$$\mathbf{x}_{dq}((k+1)\mathrm{T}) = \mathbf{G}\,\mathbf{x}_{dq}(k\mathrm{T}) + \mathbf{h}(\bullet)\,, \tag{16}$$

where $\mathbf{h}(\cdot)$ is a non-linear time-variant vector function, that is,

$$\mathbf{h}(u_d(k\mathrm{T}), u_q(k\mathrm{T}), \theta(k\mathrm{T})) = \begin{bmatrix} h_1(u_d(k\mathrm{T}), u_q(k\mathrm{T}), \theta(k\mathrm{T})) \\ h_2(u_d(k\mathrm{T}), u_q(k\mathrm{T}), \theta(k\mathrm{T})) \\ h_3(u_d(k\mathrm{T}), u_q(k\mathrm{T}), \theta(k\mathrm{T})) \\ h_4(u_d(k\mathrm{T}), u_q(k\mathrm{T}), \theta(k\mathrm{T})) \end{bmatrix}, \tag{17}$$

Note that (16), reveals that nonlinearities of the discrete state-space equation of the SVM inverter are on the function that relate the inputs with the states. It is important to note, that $\mathbf{h}(\cdot)$ depends as well as of ω, T and the initial angle θ_0 of the synchronous frame. Since these quantities are considered constant, they are not shown explicitly in (17).

In order to explore the nonlinear discrete large-signal model, next section shows the nonlinearities associated to (17), and how that non-linear function depends on the switching sequence, sampling instants and filter cut-off frequencies.

V. EXPLORING THE NON-LINEAR DISCRETE LARGE-SIGNAL MODEL

In order to understand the non-linear behavior of (16), which results from switching sequence and sampling instant, as well as the filter corner frequencies, equation (17) can be solved in each sector of the output voltage space one fundamental period. The solution of (17) has been obtained for two sampling frequency ratios m_s, ($m_s = f_s / f_1$, where f_s is the sampling frequency and f_1 is the fundamental frequency). The switching sequences for this three-phase inverter are defined in [5] and the sampling instants are shown in Fig. 8. Furthermore, the discrete control voltages $u_d(k\mathrm{T})$ and $u_q(k\mathrm{T})$ are kept constant, and the cut-frequency of the output LC filter, f_c, has been selected as 1.3kHz, and the fundamental frequency is f_1 = 60Hz. The sampling frequency and the switching frequency are equal, as in Fig. 8.

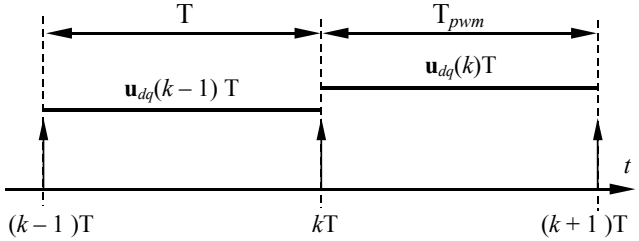

Fig. 8 – Sampling instants and control law updating.

The non-linear functions h_i together with H_i linear parameters defined in section III, are plotted in Fig. 9 and Fig. 10, for f_s equal to 10kHz and 2.5 kHz, respectively. By comparing them it is possible to conclude that as the filter corner frequencies approaches the switching frequency, the amplitude of the alternating components of $h_i(\cdot)$ increases. Among them, the 3rd

harmonic is the predominant. As a results, 2nd and 4th harmonics appears in the stationary *abc* frame, even with $u_d(k\mathrm{T})$ and $u_q(k\mathrm{T})$ constants. It has been found out that the relative amplitude of the $u_d(k\mathrm{T})$ and $u_q(k\mathrm{T})$, do not affect significantly the amplitudes of the $h_i(\cdot)$ functions. In addition, its concluded that for these switching sequences and sampling instants, the amplitude of the alternate components depend of the filter cut-off frequencies but not of the filter parameters, L and C. This is because, for the selected switching sequences and sampling instants, the inductor currents are sampled near to their average values in a sampling period, as shown in Fig. 11(c) and (d). On the other hand, the voltages are not sampled at their average values, Fig. 11(a) and (b). As a result, large low frequency components are present in the stationary *abc* frame as can be observed in the sampled line-to-line voltages, Fig. 12 (a) and (b), and in their harmonic spectrums, Fig. 12 (c) and (d), respectively. The voltages and inductor currents in rotating *dq* coordinates are presented in Fig. 13 (c)-(d) and (e)-(f) for both switching sequences, respectively. It is important to note, that this oscillation depends on the switching sequence. In addition, the sampling and control law updating are performed at the beginning of the switching period; Fig. 8 (i.e., at the zero vector) and those similar results are obtained sampling the variables and updating in the other zero vectors, Fig. 6. This results reveals that the non-linear nature of the discrete model of the space vector modulated inverter depends on the choice of the switching sequence, and sampling instants as well as the corner frequencies, demonstrating the sources of these oscillations and of the non-linear behavior the of vector function **h**(·).

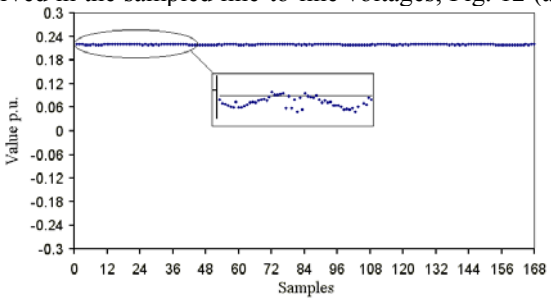

Non-linear function h_1 and linear parameter H_1

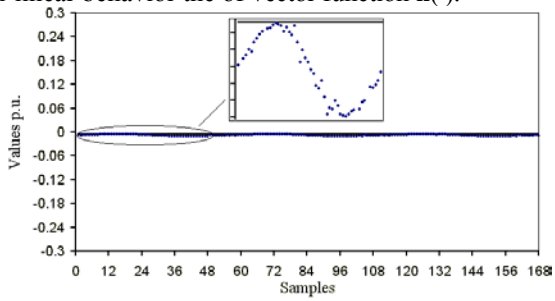

Non-linear function h_2 and linear parameter H_2

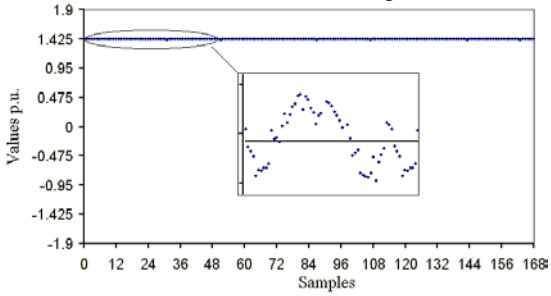

Non-linear function h_3 and linear parameter H_3

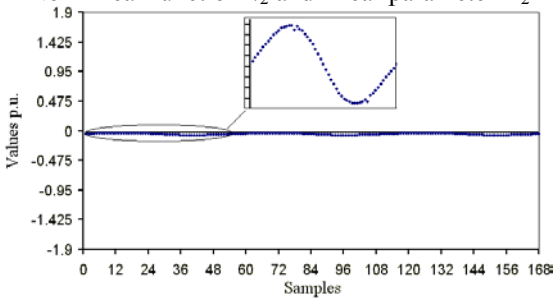

Non-linear function h_4 and linear parameter H_4

Fig. 9 – Non-linear functions *h*. and linear parameters *H*. $\boldsymbol{m_s = 168, f_s = 10\mathrm{kHz}, L = 250\mu\mathrm{H}}$ **and** $\boldsymbol{C = 60\mu\mathrm{F}, f_c = 1.3}$kHz, $\boldsymbol{u_d = 0.7071, u_q = 0}$.

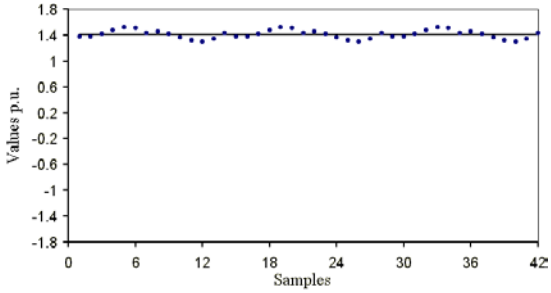

Non-linear function h_1 and linear parameter H_1

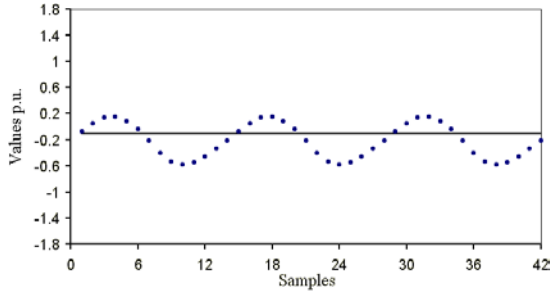

Non-linear function h_2 and linear parameter H_2

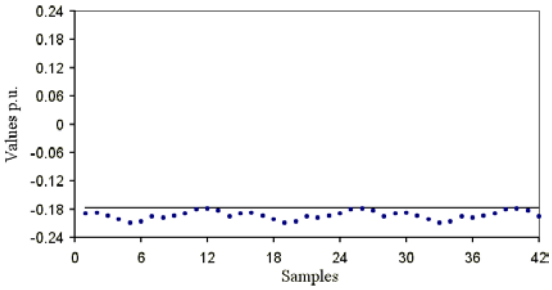

Non-linear function h_3 and linear parameter H_3

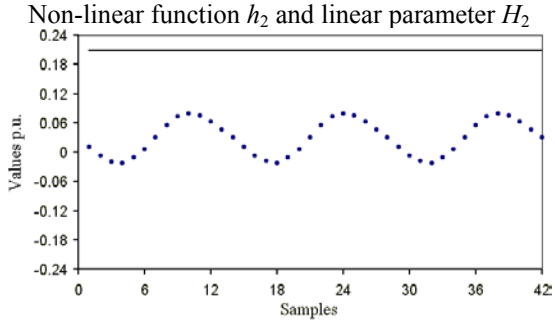

Non-linear function h_4 and linear parameter H_4

Fig. 10 – Non-linear functions *h*. and linear parameters *H*. $\boldsymbol{m_s = 42, f_s = 2.5\mathrm{kHz}, L = 250\mu\mathrm{H}}$ **and** $\boldsymbol{C = 60\mu\mathrm{F}, f_c = 1.3\mathrm{kHz}, u_d = 0.7071, u_q = 0}$.

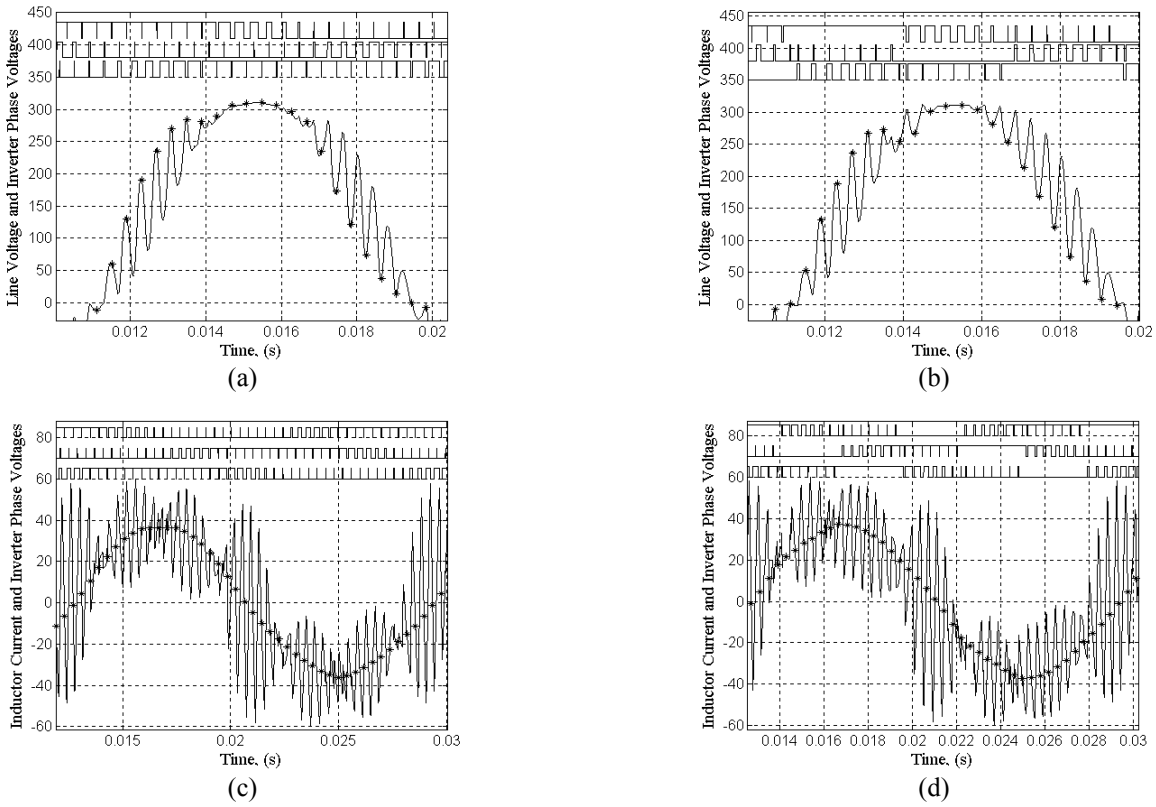

Fig. 11 – Simulation results. Line-to-line voltage v_{ab}, and inductor current i_a. (a), (c) Shows the line-to-line voltage for one symmetric switching sequence, and (b), (d) shows the same voltage and current for other symmetric switching sequence. The sampling frequency is equal to the switching frequency and the sampling and control law updated is performed at the beginning of the sampling period The filter parameters are $\boldsymbol{L = 250\mu H}$, $\boldsymbol{C = 60\mu F}$. $\boldsymbol{m_s = 42}$, $\boldsymbol{f_s = 2.5kHz}$, $\boldsymbol{f_c = 1.3kHz}$. $\boldsymbol{u_d = 0.7071}$, $\boldsymbol{u_q = 0}$.

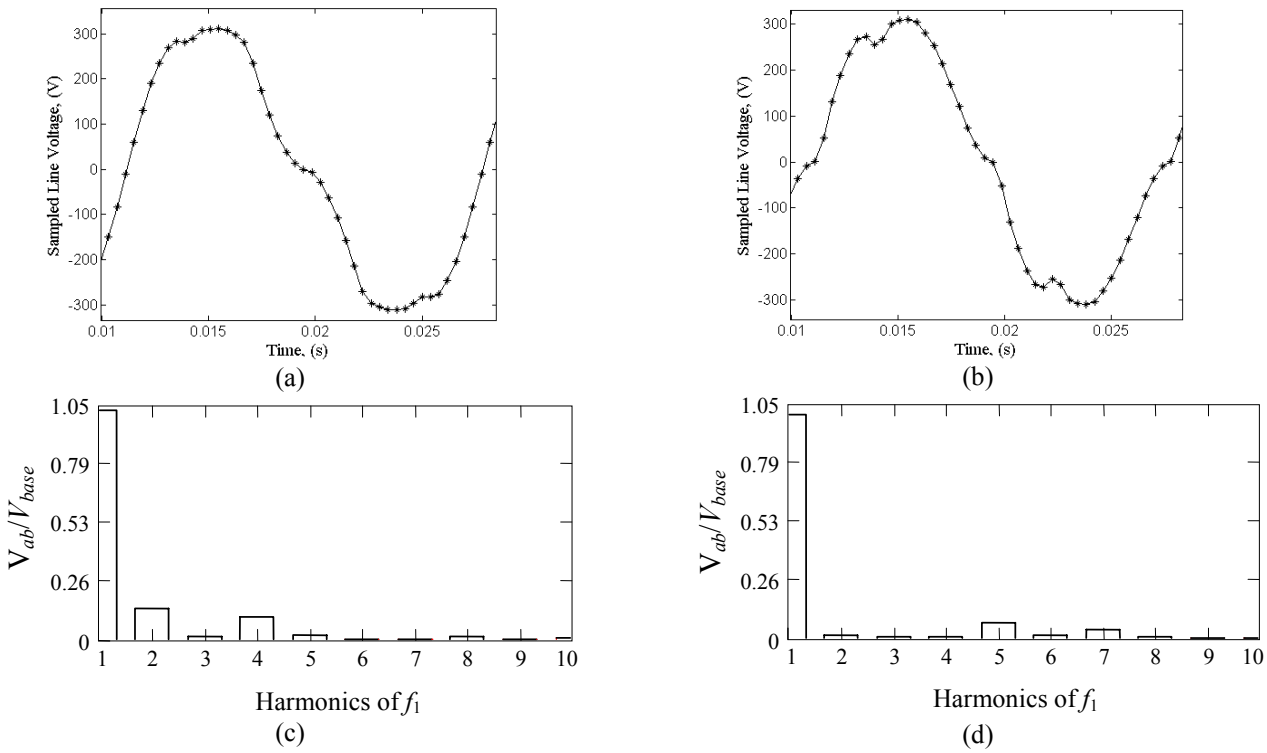

Fig. 12 – Simulation results. (a) and (b), shows the sampled line-to-line output voltage v_{ab}, for two switching sequences shown in Fig. 11. (c) and (d), shows the harmonic spectrum presented in the line-to-line output voltage for both cases.

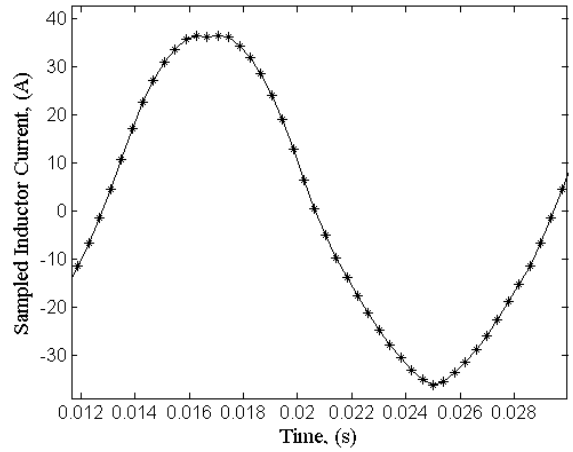

(a)

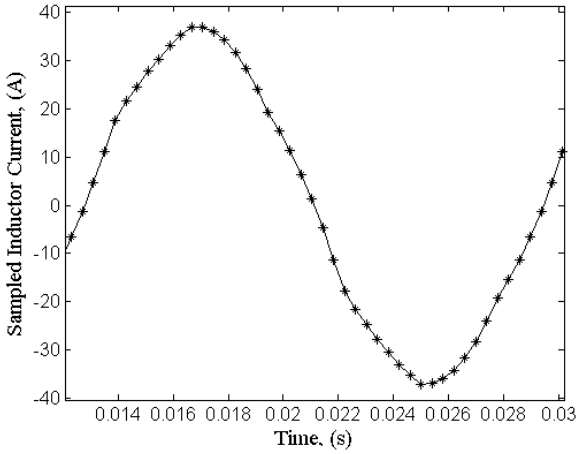

(b)

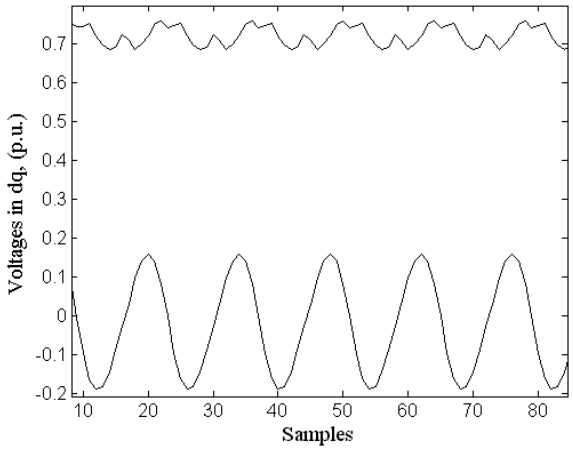

(c). Voltages in *dq* rotating frame.

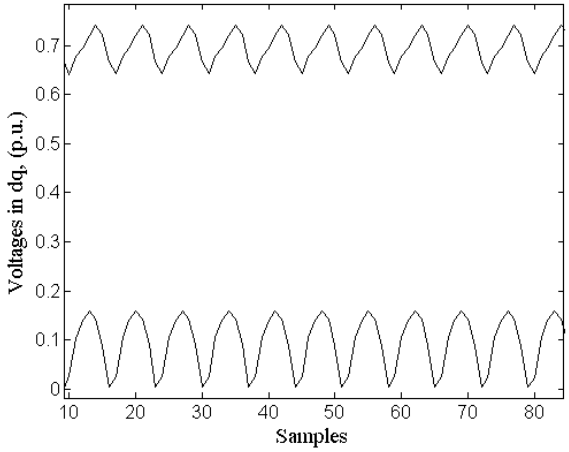

(d). Voltages in *dq* rotating frame.

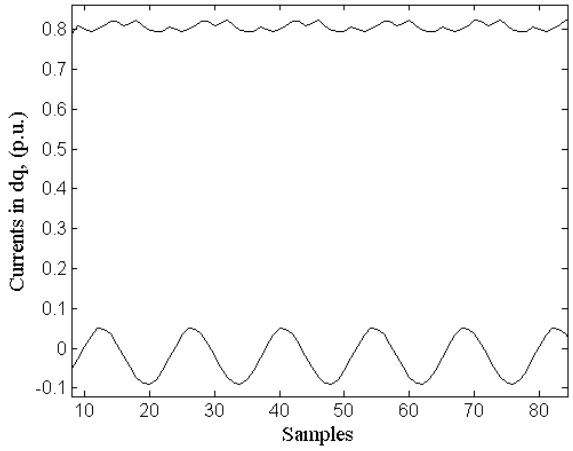

(e). Currents in *dq* rotating frame.

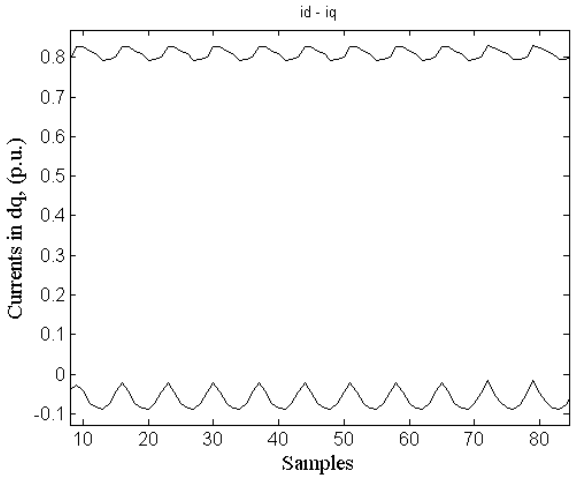

(f) Currents in *dq* rotating frame.

Fig. 13 – Simulation results. (a), (c) and (e), shows the sampled inductor current i_a, dq voltages and *dq* currents for one switching sequence. The oscillation is at 180 Hz in figure (c) and (e). On the other hand, (b), (d) and (f), shows similar variables for the second sequence. The oscillation frequency is of 300 Hz in figure (d) and (f). The filter parameters are $\boldsymbol{L = 250\mu H}$, $\boldsymbol{C = 60\mu F}$. $\boldsymbol{m_s = 42}$, $\boldsymbol{f_s = 2.5kHz}$, $\boldsymbol{f_c = 1.3kHz}$. $\boldsymbol{u_d = 0.7071}$, $\boldsymbol{u_q = 0}$.

VI. IMPACT OF THE SAMPLING INSTANTS

In this section are presents two possible solutions to reduce the amplitudes of the low order harmonics in sampled variables.

With loss of generality, let us consider that in all cases the filter parameters are, L = 250μH, C = 60μF, f_c = 1.3kHz. Switching frequency is 2.5kHz and the discrete control actions are, $u_d = 0.7071$, $u_q = 0$.

Method A:

In this method, the sampling and the control law updating are performed twice in a switching period, as shown in Fig. 14 that is, the sampling frequency is f_s = 5kHz.

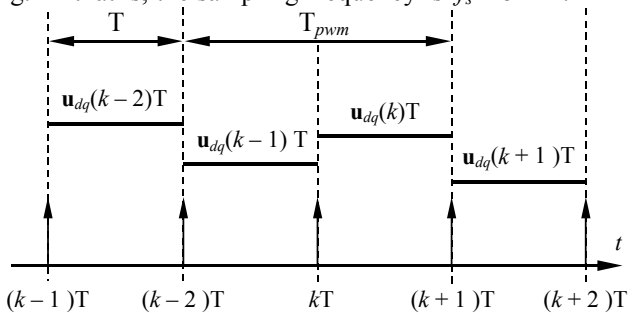

Fig. 14 – Sampling instants and control law updating. *Method A*.

The phase voltage v_{ab} and inductor current i_a, are shown in Fig. 15, where also are shown the three-phase PWM voltages produced by the inverter. The (*) in Fig. 18(a) and (b), indicates the instants when the variable is sampled. Fig. 16(a) shows the sampled output voltage v_{ab} and Fig. 16(b) the harmonic spectrum of this voltage, and Fig. 17, the voltages and currents in rotating *dq* frame.

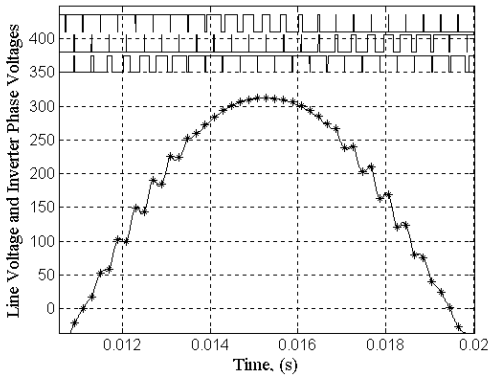

(a)

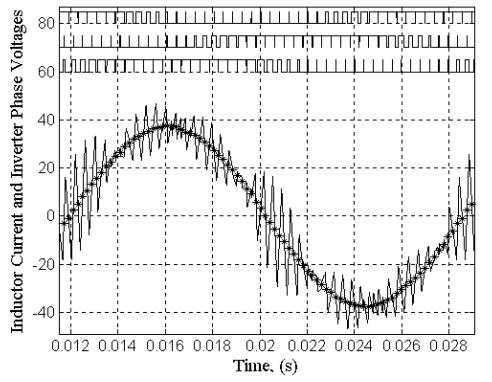

(b)

Fig. 15 – Simulation Results. (a) Line-to-line voltage v_{ab}, and (b) Inductor current i_a. PWM phase voltages produced by the inverter.

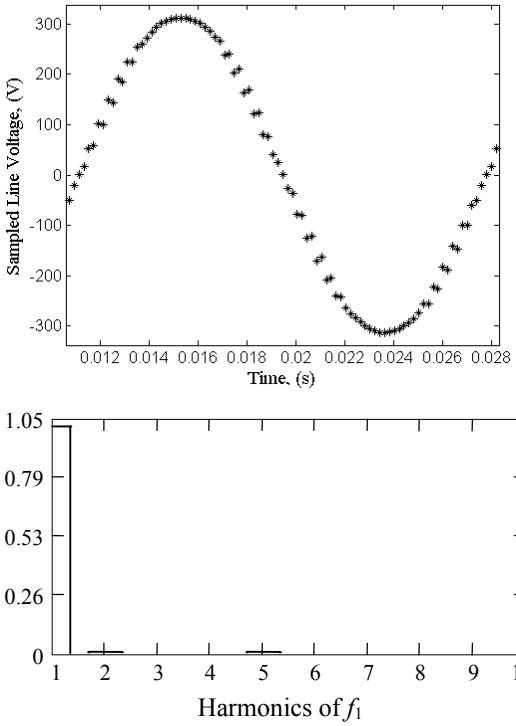

Fig. 16 – Simulation Results. (a) Sampled line-to-line voltage v_{ab}, (b) Harmonic spectrum presented in the sampled output voltages.

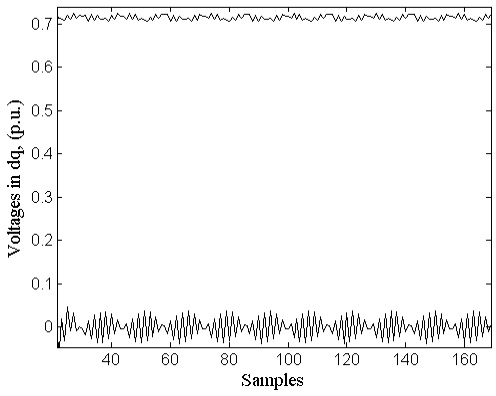

(a)

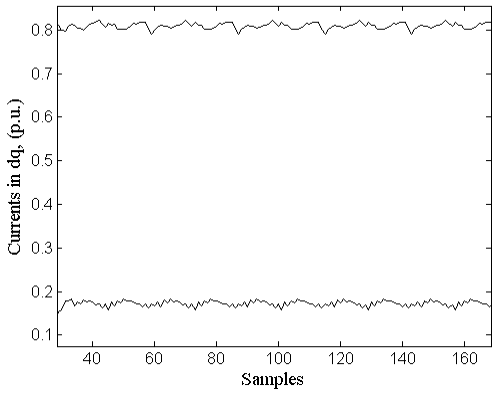

(b)

Fig. 17 – Simulation results. (a) Shows the voltages in rotating *dq* frame. (b) Currents in rotating *dq* frame. The low oscillations are at 360 Hz and the higher are at the half of switching frequency.

Method B:

In this method, the sampling is performed twice in a switching period, while the control law updating only once, as shown in Fig. 18. The average of this sampled values are used to compute the control law. Switching frequency is 2.5kHz, and sampling frequency, f_s = 5kHz.

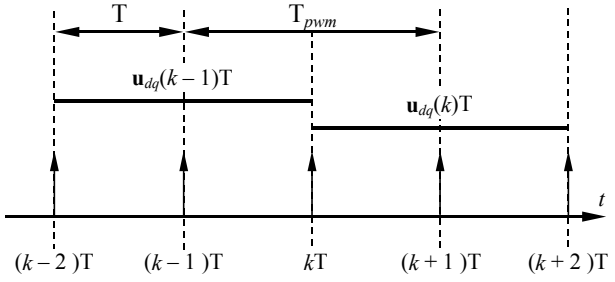

Fig. 18 – Sampling instants and control law updating. *Method B*.

The phase voltage v_{ab} and inductor current i_a, resulting of this method, are presented in Fig. 19(a) and (b), where also are shown the three-phase PWM voltages produced by the inverter. The (*) in Fig. 19(a) and (b) represents the average of the two last samples. Fig. 20(a) shows the average sampled output voltage v_{ab} and Fig. 20 (b) the harmonic spectrum of this voltage. In addition, Fig. 21, the voltages and currents in rotating dq frame.

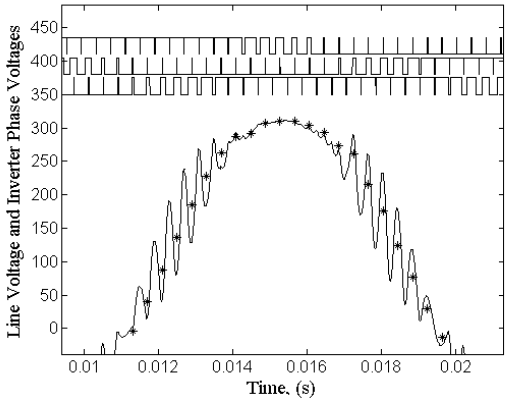

(a)

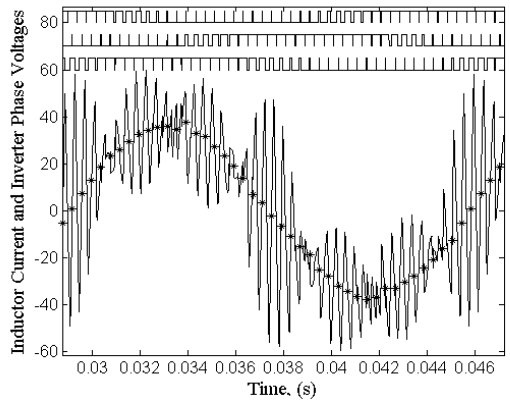

(b)

Fig. 19 – Simulation Results. (a) Line-to-line voltage v_{ab}, and inductor current i_a. PWM phase voltages produced by the inverter.

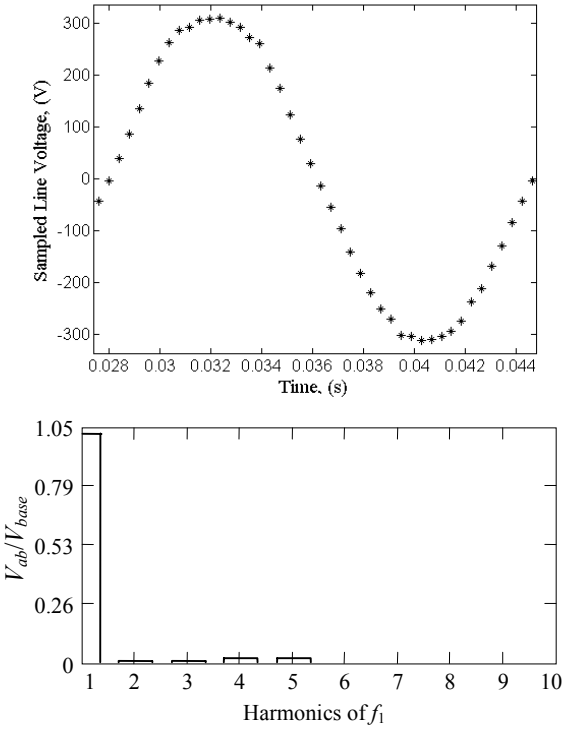

Fig. 20 – Simulation Results. (a) Average sampled line voltage v_{ab}, (b) Harmonic spectrum presented in the sampled output voltages.

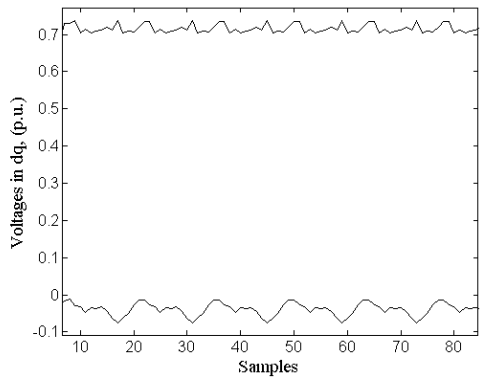

(a)

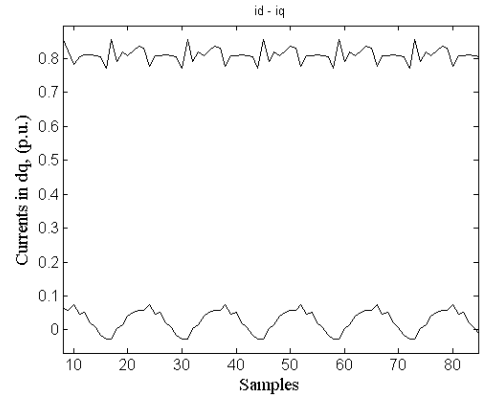

(b)

Fig. 21 – Simulation results. (a) and (b), shows the voltages and currents in rotating dq frame respectively. The oscillation is at the low frequency of 180 Hz

The Method A requires a computational effort greater than the Method B. Both methods reduce significantly the low order harmonic content if compared with the method of Fig. 8, and the harmonic spectrum of the output line voltages of Method A, Fig. 16, it is enhanced regarding the other ones two. On the other hand, the variables in rotating *dq* frame have high frequencies oscillations at the half sampling frequency. But is possible to see that the ripple over the inductor currents is reduced in the Method A, Fig. 15, is compared with the others two. Furthermore, the computational effort is reduced in Method B, since the additional sample does not increase significantly the CPU overhead and the variables in rotating *dq* frame appear without high frequency oscillations. Finally, the method depicted in Fig. 8 requires a least computational effort being more to adequate for high switching frequencies, since in these cases there are small output voltage and current ripples.

VII. IMPROVED DISCRETE MODEL

This section proposes an improved model that allows to carry out the controllers design using linear time-invariant systems techniques. Starting from the nonlinear model, proposed in Section IV, it is possible to obtain a linear approximated model. This model, can be obtained computing the $h(\cdot)$ functions (17) for different pairs of $[u_d(k\mathrm{T}),u_q(k\mathrm{T})]$ in one fundamental period, in a such way to consider all the possible operating points of the three-phase inverter. Then, a least square approximation of the average value of the each nonlinear function $h_i(\cdot)$ over the fundamental period can be obtained, that is,

$$\begin{bmatrix} h_1(\bullet) \\ h_2(\bullet) \\ h_3(\bullet) \\ h_4(\bullet) \end{bmatrix} \approx \begin{bmatrix} \overline{h}_1 \\ \overline{h}_2 \\ \overline{h}_3 \\ \overline{h}_4 \end{bmatrix} \text{ where, } \begin{matrix} \overline{h}_1 = [\overline{h}_{11} \quad \overline{h}_{12}][u_d \quad u_q]^{\mathrm{T}} \\ \overline{h}_2 = [\overline{h}_{21} \quad \overline{h}_{22}][u_d \quad u_q]^{\mathrm{T}} \\ \overline{h}_3 = [\overline{h}_{31} \quad \overline{h}_{32}][u_d \quad u_q]^{\mathrm{T}} \\ \overline{h}_4 = [\overline{h}_{41} \quad \overline{h}_{42}][u_d \quad u_q]^{\mathrm{T}} \end{matrix},$$

where, the h_{ij} are the parameters of a linear model result of the lower sum of the square errors in one fundamental period.

In Fig. 22 are shown two linear approximated models, in this case only for h_1, h_2 functions, and H_1, H_2 parameters, since the others appear similar. The first one is the average model obtained in the Section III, and the second is the described above. These linear models have been obtained for m_s of 168 and 42. For large values of m_s, these models converge, however, for lower values of m_s, the proposed least square based model results in a better approximation since it results in a lower sum of the square errors.

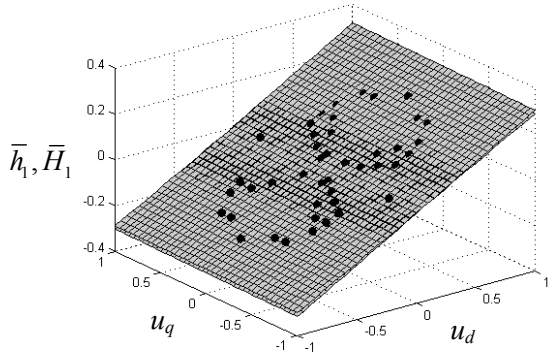

(a). Average of the function h_1 and parameters H_1.

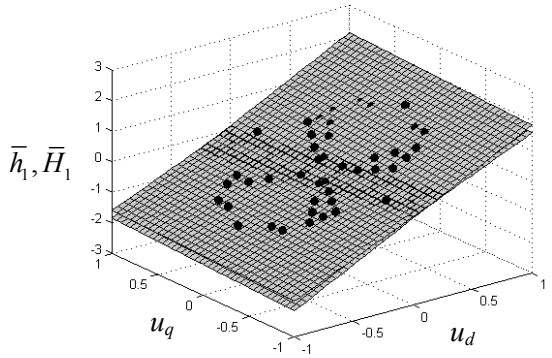

(b). Average of the function h_1 and parameters H_1.

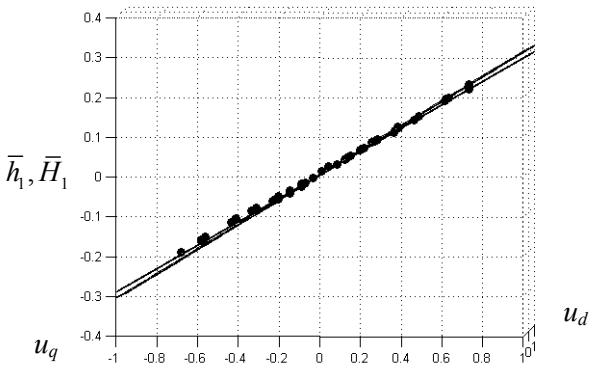

(c). Average of the function h_1 and parameters H_1.

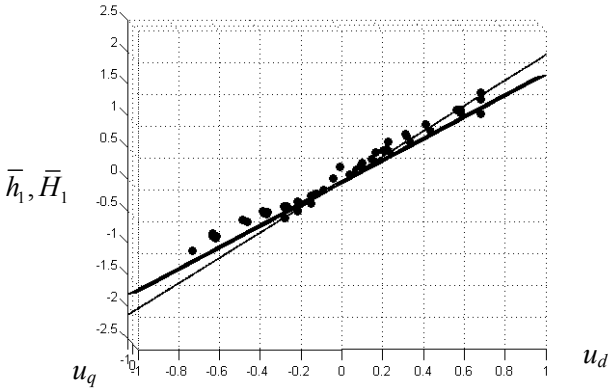

(d). Average of the function h_1 and parameters H_1.

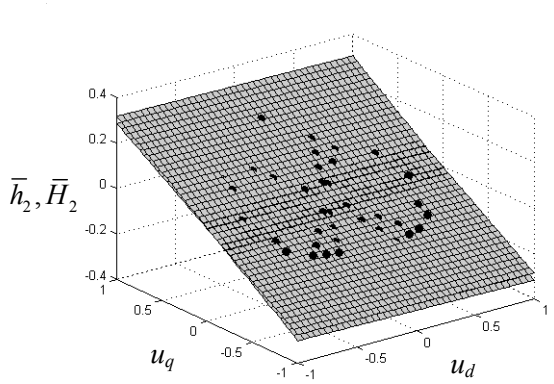

(e). Average of the function h_2 and parameters H_2.

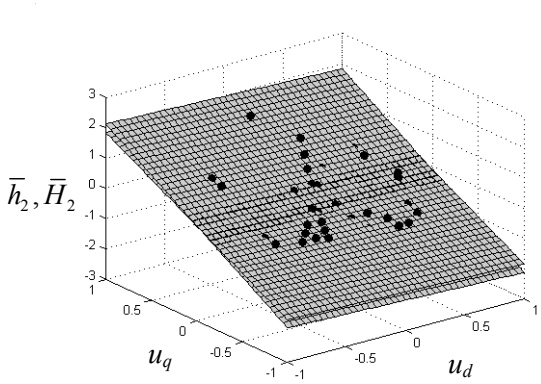

(f). Average of the function h_2 and parameters H_2.

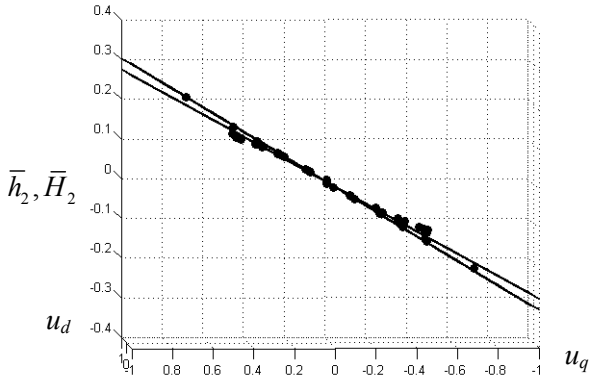

(g). Average of the function h_2 and parameters H_2.

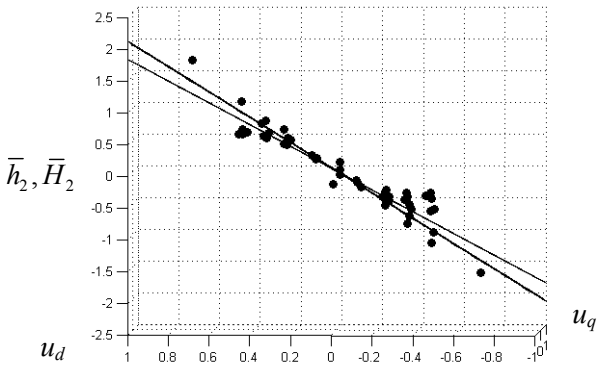

(h). Average of the function h_2 and parameters H_2.

Fig. 22 – Comparison of the average discrete non-linear large-signal model $h_i(\cdot)$ and the average discrete (ZOH) linear model H_i. (a), (c), (e), (g), $\boldsymbol{m_s = 168}$, $\boldsymbol{f_s = 10kHz}$. (b), (d), (f), (h), $\boldsymbol{m_s = 42}$, $\boldsymbol{f_s = 2.5kHz}$.

SUMMARY

This paper proposes a large-signal discrete non-linear model for a voltage-fed space vector modulated three-phase inverter in rotating *dq* coordinates. This model consider the ripple over the variables of the interest as well as takes into account the impact of the switching sequence, sampling instants and corner frequencies. It is found out that as the switching frequency increase with respect to the filter corner frequency, ZOH average model converges to the average model obtained from the non-linear time-variant large-signal model. However, if the assumptions made for the ZOH average model are violated, an improved discrete nonlinear model, should be considered to describe the relationship between the input and outputs of the three-phase space vector modulated inverter in rotating frame. It has been found out, that the selection of the appropriate sampling instant and switching sequence, can be to reduce the low order harmonics in the sampled variables when the filter corner frequencies approaches the switching frequency.

ACKNOWLEDGEMENT

The authors would like to thanks FAPERGS, CAPES and CNPq for the financial support.

REFERENCES

[1] H. W. Van Der Broeck, H. C. Skudelny and G. V. Stanke, "Analysis and realization of a pulsewidth modulator based on voltage space vectors", *IEEE Trans. Ind. Applicat.*, v. 24, pp. 142–150, Jan./Feb. 1988.

[2] V. T. Ranganathan, "Space vector pulsewidth modulation – A status review", *Sãdhanã*, v. 22, pp. 675–688, Dec. 1997.

[3] L. Huber and D. Boroyevich, "Space vector modulated three-phase to three-phase matrix converter with input power factor correction", *IEEE Trans. Industry Applications*, v. 31, pp. 1234–1246, Nov./Dec. 1995.

[4] H. Pinheiro, R. Blume and P. Jain, "Space vector modulation method for single-phase on-line three-leg UPS", in *IEEE INTELEC Conf. Proc.*, pp. 679–686, 2000.

[5] H. Pinheiro, F. Botterón, C. Rech, L. Schuch, R. F. Camargo, H. L. Hey, H. A. Grundling, J. R. Pinheiro; "Space vector modulation for voltage-source inverters: a unified approach", *IEEE IECON Conf. Proc.*, vol. 1, pp. 23–29, 2002.

[6] Khai D. T. Ngo, "Low frequency characterization of PWM converters", *IEEE Trans. on Power Electronics*, vol. PE-1, no. 4, pp. 223-230, Oct 1986.

[7] Rim C. T., Hu D. Y., Cho G. H., "Transformers as Equivalent Circuits for Switches: General Proofs and D-Q Transformation-Based Analysis", *IEEE Trans. on Industry Applic.*, vol. 26, no. 4, pp. 777-785, Jul/Ago 1990.

[8] Silva H., Boroyevich D., Cuadros C., "Small-signal modeling and control of three-phase PWM converters", *IEEE Industry Applications Society Ann. Meet.*, *Conf. Proc.*, vol.2, pp. 1143 – 1150, 1994.

[9] Silva H., and Boroyevich D., "Small-Signal Modeling of Three-Phase PWM Modulators" *IEEE Power Electronics Specialist Conference*, *Conf. Proc.*, vol. 1, pp. 550–555, 1996.

[10] H. Mao, D. Boroyevich, F. C. Y. Lee, "Novel Reduced-Order Small-Signal Model of a Three-Phase PWM Rectifier and its Application in Control Design and System Analysis", *IEEE Trans. on Power Electronics*, vol. 13, no. 3, pp. 511-521, May 1998.

[11] J. Holtz, "Pulsewidth Modulation – A Survey", *IEEE Trans. on Ind. Electronics.*, vol. 39, no. 5, pp. 410-420, Dec 1992.
[12] Kawabata, T., Miyashita T., Yamamoto Y., "Digital Control of Three-Phase PWM Inverter with LC Filter", *IEEE Trans. on Power Electronics*, vol. 6, no. 1, pp. 62-72, Jan 1991.
[13] Ito Y., Kawauchi, S., "Microprocessor-Based Robust Digital Control for UPS with Three-Phase PWM Inverter", *IEEE Trans. on Power Electronics*, vol. 10, no. 2, pp. 196-204, March 1995.
[14] Kukrer, O.; "Discrete-Time Current Control of Voltage-Fed Three-Phase PWM Inverters", *IEEE Trans. on Power Electronics*, vol. 11, no. 2, pp. 260-269, March 1996.
[15] Choi J-W., Sul S-K., "Fast Current Controller in Three-Phase AC/DC Bosst Converter Using *d-q* Axis Crosscoupling", *IEEE Trans. on Power Electronics*, vol. 13, no. 1, pp. 179-185, Jan 1998.
[16] Botterón, F.; Pinheiro, H.; Grundling, H.A.; Pinheiro, J.R.; Hey, H.L., "Digital voltage and current controllers for three-phase PWM inverter for UPS applications", *IEEE Industry Applications IAS Annual Meeting Conf. Proc.*, vol. 4, pp. 2667-2674, 2001.
[17] Cho J-S; Lee S-Y; Mok H-S; Choe G-H; "Modified deadbeat digital controller for UPS with 3-phase PWM inverter"; *IEEE Industry Applications Conference IAS Annual Meeting Conf. Proc.*, vol. 4, pp. 2208-2215, 1999.
[18] Blasko, V.; Kaura, V.; Niewiadomski, W.; "Sampling methods for discontinuous voltage and current signals and their influence on bandwidth of control loops of electrical drives"; *Applied Power Electronics Conference and Exposition, Conf. Proc.*, vol. 1, pp. 520-526, Feb. 1997.
[19] Song S-H., Choi J-W., Sul S-K., "Current Measurements in Digitally Controlled AC Drives", *IEEE Industry Applications Magazine*, pp. 51-62, 2000.

APPENDIX

The matrices **A**, **B** and **F** of the state-space model of LC filter and load in equation (1), are:

$$\mathbf{A}=\begin{bmatrix} 0 & 0 & 0 & -\frac{2}{3L_o} & \frac{1}{3L_o} & \frac{1}{3L_o} \\ 0 & 0 & 0 & \frac{1}{3L_o} & -\frac{2}{3L_o} & \frac{1}{3L_o} \\ 0 & 0 & 0 & \frac{1}{3L_o} & \frac{1}{3L_o} & -\frac{2}{3L_o} \\ \frac{1}{C} & 0 & 0 & 0 & 0 & 0 \\ 0 & \frac{1}{C} & 0 & 0 & 0 & 0 \\ 0 & 0 & \frac{1}{C} & 0 & 0 & 0 \end{bmatrix},\ \mathbf{B}=\begin{bmatrix} \frac{2}{3L_o} & \frac{1}{3L_o} \\ -\frac{1}{3L_o} & \frac{1}{3L_o} \\ -\frac{1}{3L_o} & -\frac{2}{3L_o} \\ 0 & 0 \\ 0 & 0 \\ 0 & 0 \end{bmatrix},\ \mathbf{F}=\begin{bmatrix} 0 & 0 & 0 \\ 0 & 0 & 0 \\ 0 & 0 & 0 \\ -\frac{1}{C} & 0 & 0 \\ 0 & -\frac{1}{C} & 0 \\ 0 & 0 & -\frac{1}{C} \end{bmatrix}. \quad \text{(A1)}$$

The linear transformations used to transform the three-phase systems to stationary αβ coordinates, is given by (A2),

$$\mathbf{T}_{\alpha\beta}=\sqrt{\frac{2}{3}}\begin{bmatrix} 1 & -\frac{1}{2} & -\frac{1}{2} \\ 0 & \frac{\sqrt{3}}{2} & -\frac{\sqrt{3}}{2} \end{bmatrix}, \quad \text{(A2)}$$

and the linear transformation that transform the system in the αβ coordinates to the rotating *dq* frame, is given by (A3).

$$\mathbf{T}_{dq}(t)=\begin{bmatrix} \cos(\theta(t)) & \text{sen}(\theta(t)) \\ -\text{sen}(\theta(t)) & \cos(\theta(t)) \end{bmatrix}. \quad \text{(A3)}$$

The matrices of state-space equation of the large signal linear model in rotating *dq* frame are given by

$$\mathbf{A}_{dq}=\begin{bmatrix} 0 & \omega & \frac{1}{C} & 0 \\ -\omega & 0 & 0 & \frac{1}{C} \\ -\frac{1}{L_o} & 0 & 0 & \omega \\ 0 & -\frac{1}{L_o} & -\omega & 0 \end{bmatrix},\ \mathbf{B}_{dq}=\begin{bmatrix} 0 & 0 \\ 0 & 0 \\ \frac{1}{L_o} & 0 \\ 0 & \frac{1}{L_o} \end{bmatrix},\ \mathbf{F}_{dq}=\begin{bmatrix} -\frac{1}{C} & 0 \\ 0 & -\frac{1}{C} \\ 0 & 0 \\ 0 & 0 \end{bmatrix}, \quad \text{(A4)}$$

where "ω" is the desired output frequency.